

CHROM. 18 506

NEW ANGLE ROTOR COIL PLANET CENTRIFUGE FOR COUNTER-CURRENT CHROMATOGRAPHY

I. ANALYSIS OF ACCELERATION

YOICHIRO ITO

National Heart, Lung, and Blood Institute, Laboratory of Technical Development, Building 10, Room 5D-12, Bethesda, MD 20892 (U.S.A.)

(Received January 27th, 1986)

SUMMARY

Simple mathematical analysis has been performed on a new type of synchronous planetary motion to elucidate the acceleration field. Using generalized formulae derived from the above analysis, distribution of the centrifugal force vectors produced by all types of the synchronous planetary motion is computed and expressed in the same format to facilitate comparative studies. The results of the above analysis predict high performance of the new angle rotor coil planet centrifuge in counter-current chromatography.

INTRODUCTION

In the past, various types of rotary-seal-free flow-through centrifuges have been designed for performing counter-current chromatography (CCC) and cell elutriation¹. Among these, a particular group of coil planet centrifuges which provide synchronous planetary motion of the column holder has proven most useful. Four types of these synchronous flow-through coil planet centrifuges are schematically illustrated in the left-hand column of Fig. 1, where each diagram indicates orientation and motion of a cylindrical holder with a bundle of flow tubes for continuous elution. In Scheme I planetary motion, the vertical holder revolves around the central axis of the centrifuge at angular velocity ω while it simultaneously counter-rotates around its own axis at the same angular velocity. As described earlier^{1,2}, this counter-rotation of the holder steadily unwinds the twist of the tube bundle caused by the revolution, thus eliminating the need for the conventional rotary seals. This twist-free mechanism works equally well in other synchronous schemes with tilted (Scheme II), horizontal (Scheme III) or even inverted (Scheme IV) orientation of the holder.

Analyses of acceleration produced by these synchronous planetary motions have been performed on Schemes I, III and IV, revealing a characteristic centrifugal force field inherent to each scheme. The two typical synchronous planetary motions, Schemes I and IV, produce relatively simple centrifugal force fields, which are always

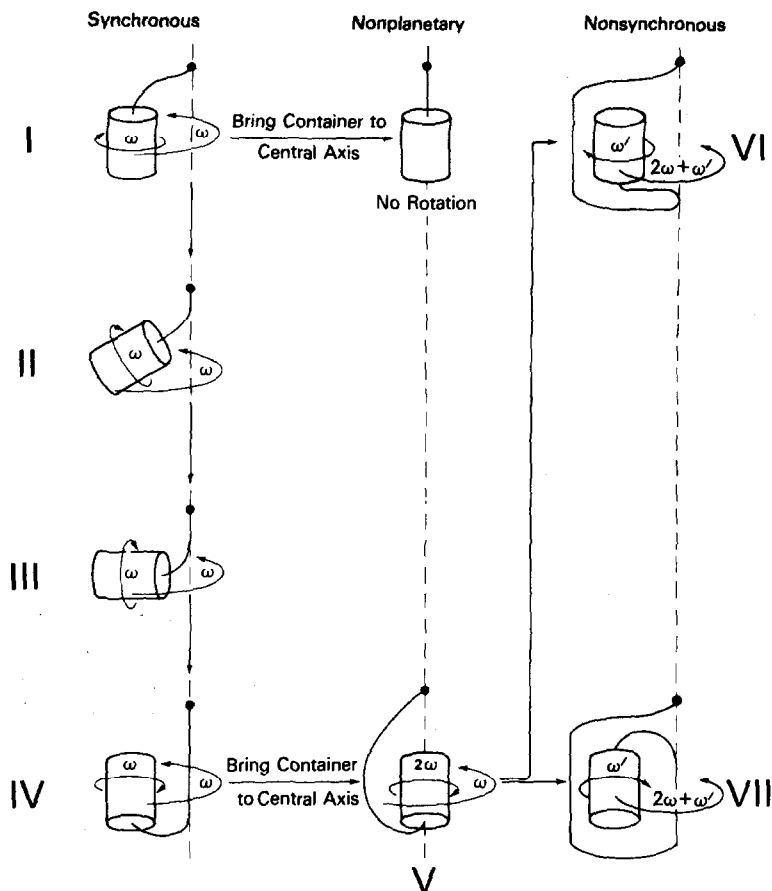


Fig. 1. Various types of flow-through centrifuge systems free of rotary seals. In order to provide room for the new synchronous planetary motion introduced in this paper, more descriptive new nomenclature is proposed, as indicated in Fig. 6.

confined in a plane perpendicular to the holder axis. However, despite their apparent similarity in the planetary motion, centrifugal force fields produced by these two schemes are quite different. The Scheme I planetary motion produces homogeneous distribution of centrifugal force vectors for every point on the holder while the force field rotates around each point at a rate equal to the revolution of the holder. On the other hand, the Scheme IV planetary motion displays a more complex distribution pattern of the centrifugal force vectors, which vary in both magnitude and direction according to the location of the point on the holder. Each vector also undergoes periodic change during each revolutional cycle. Previous studies have shown that these two different force fields produce contrasting hydrodynamic effects on the two immiscible solvent phases in the coiled column. The Scheme I planetary motion tends to distribute two solvent phases rather evenly from one end of the coil, called the head, and any excess of either phase is accumulated at the other end, called the tail. (The head-tail relationship of a rotating coil is determined by the Archimedean screw

force which tends to drive all objects from the tail toward the head.) In the Scheme IV planetary motion, the two solvent phases are unevenly distributed through the coil and often completely separated along the length of the coil, one phase entirely occupying the head and the other phase the tail of the coil. This unilateral hydrodynamic distribution is unique to this Scheme IV planetary motion and has proven extremely useful for performing CCC.

The Scheme III planetary motion displays the most complex pattern of the centrifugal force field, which undergoes three-dimensional fluctuation. However, except for the location remote from the holder axis, the centrifugal force dominantly acting along the holder axis toward the periphery provides stable retention of the stationary phase even for the aqueous-aqueous polymer phase systems having a high tendency of emulsification. Analyses of acceleration produced by the Scheme II planetary motion have not been reported, but the system is considered to be the hybrid of Schemes I and III where inclination of the holder determines the degree of mixing and retention of the solvents. In fact, the optimum holder angle has been experimentally determined to be around 30° from the vertical line³.

Observation of the diagram (Fig. 1), from Schemes I-IV, clearly indicates that another hybrid scheme should be present between Schemes III and IV to complete the illustration of the synchronous planetary motions. A great contrast between Schemes I and IV in their centrifugal force field strongly suggests that this new hybrid scheme will produce a novel pattern of the centrifugal force field.

In the present paper, a simple mathematical analysis has been performed on the synchronous planetary motion of this new hybrid scheme. By the use of a set of generalized formulae derived for acceleration analysis, distribution of the centrifugal force vectors for each scheme is diagrammatically expressed in the same format for comparative studies on all types of synchronous planetary motions.

ANALYSIS OF ACCELERATION

We consider a discoid body with radius r and its axis being held at angle Ψ from the central axis of the stationary frame (Fig. 2). The discoid body undergoes a synchronous planetary motion in such a way that it revolves around the central axis at an angular velocity, ω , with a revolutional radius, R , and simultaneously rotates about its own axis at the same angular velocity. Then, we wish to study the motion of an arbitrary point present on the periphery of the discoid body.

Fig. 3A shows an x - y - z coordinate system where the center of the discoid body initially locates at point $Q_0(R, 0, 0)$ and the arbitrary point at $P_0(R - r \cos \Psi, 0, r \sin \Psi)$. The center of the discoid body circles around point 0 in the x - y plane and at time t moves angle $\theta = \omega t$ to reach point $Q(R \cos \theta, R \sin \theta, 0)$. By the aid of a diagram illustrated in Fig. 3B, the location of the arbitrary point on the discoid body is expressed by $P(x, y, z)$ according to the following equations:

$$x = R \cos \theta + r[1 - (1 + \cos \Psi) \cos^2 \theta] \quad (1)$$

$$y = R \sin \theta - r(1 + \cos \Psi) \sin \theta \cos \theta \quad (2)$$

$$z = r \sin \Psi \cos \theta \quad (3)$$

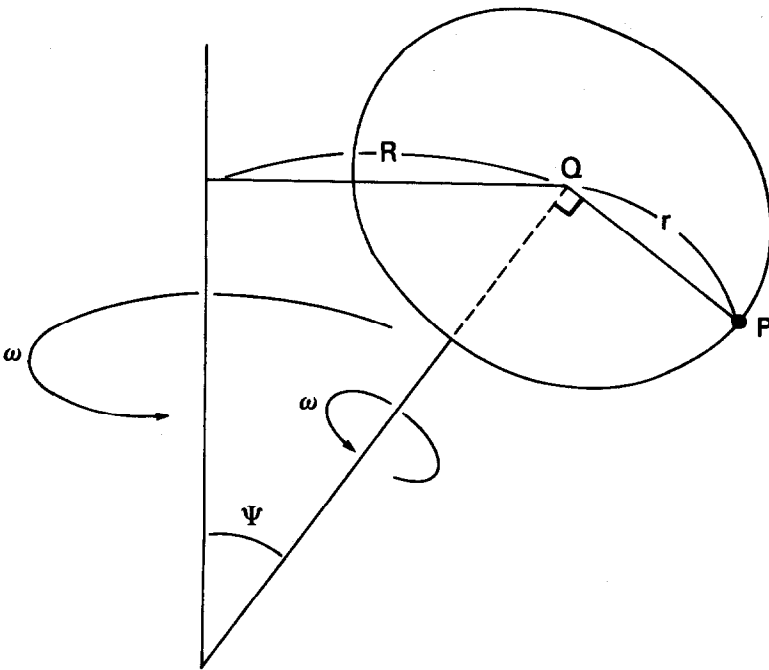


Fig. 2. Synchronous planetary motion of the discoid body.

where R is the distance \overline{OQ} ; r , the distance \overline{QP} ; and Ψ , the angle formed between the z -axis and the body axis, \overline{QA} .

The acceleration, α , produced by the planetary motion is then computed from the second derivatives of the above equations as

$$\alpha_x = d^2x/dt^2 = -R\omega^2 [\cos \theta - 2\beta (1 + \cos \Psi) \cos 2\theta] \quad (4)$$

$$\alpha_y = d^2y/dt^2 = -R\omega^2 [\sin \theta - 2\beta (1 + \cos \Psi) \sin 2\theta] \quad (5)$$

$$\alpha_z = d^2z/dt^2 = -r\omega^2 \sin \Psi \cos \theta \quad (6)$$

where $\beta = r/R$ and $R \neq 0$. Using eqns. 4-6, the x , y , z components of the acceleration vector can be computed and displayed separately or in a combined form in the x - y - z coordinate system of the stationary reference frame.

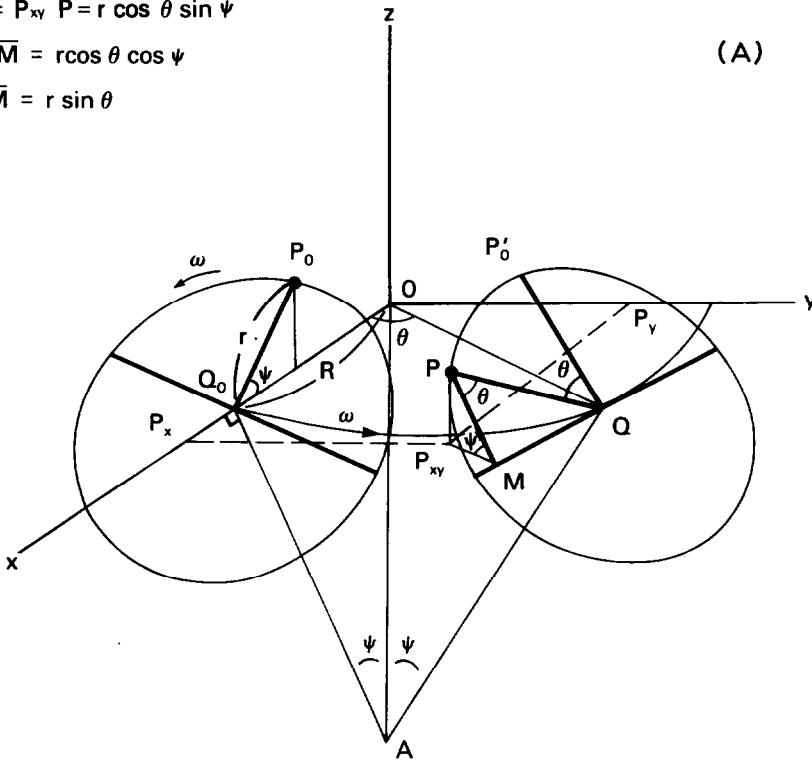
However, the effects of the acceleration on the subjects moving with the discoid body can be more effectively visualized if the acceleration is expressed with respect to the revolving body frame. Fig. 4 shows the relationship between the original x - y - z coordinate system and the x_b - y_b - z_b body coordinate system in which the z_b -axis coincides with the axis of the discoid body. The x_b - y_b - z_b coordinate system revolves around the z -axis of the original coordinate system in such a way that the

$$Z = \overline{P_{xy}} \overline{P} = r \cos \theta \sin \psi$$

$$\overline{P_{xy}} \overline{M} = r \cos \theta \cos \psi$$

$$\overline{QM} = r \sin \theta$$

(A)



$$x = \overline{OP_x} = \overline{OQ_x} + \overline{Q_xM_x} - \overline{P_xM_x}$$

$$\overline{OQ_x} = R \cos \theta$$

$$\overline{Q_xM_x} = \overline{QM} \sin \theta = r \sin^2 \theta$$

$$\overline{P_xM_x} = \overline{P_xM} \cos \theta = r \cos^2 \theta \cos \psi$$

$$y = \overline{OP_y} = \overline{OQ_y} - \overline{M_yQ_y} - \overline{P_yM_y}$$

$$\overline{OQ_y} = R \sin \theta$$

$$\overline{M_yQ_y} = \overline{QM} \cos \theta = r \sin \theta \cos \theta$$

$$\overline{P_yM_y} = \overline{P_yM} \sin \theta = r \cos \theta \sin \theta \cos \psi$$

(B)

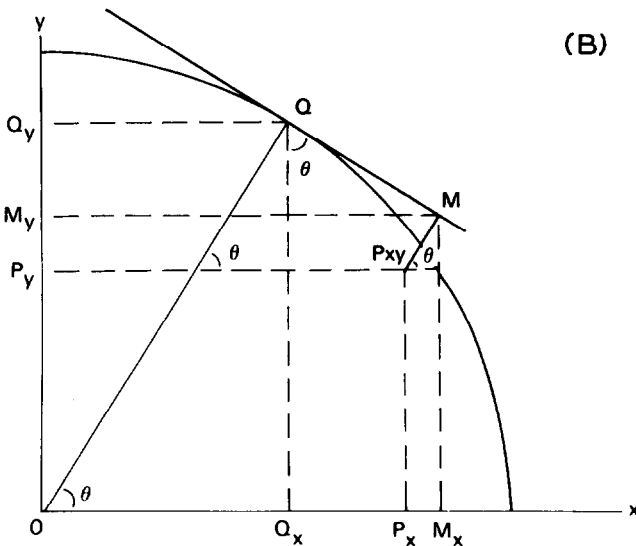


Fig. 3. Coordinate systems for analysis of acceleration. (A) x - y - z coordinate system; (B) x - y coordinate system for assisting the analysis.

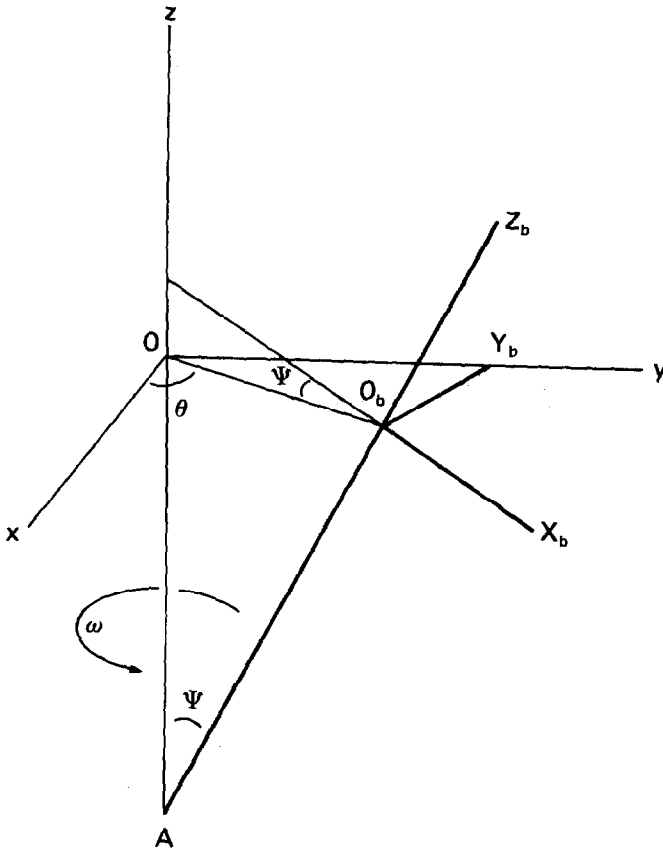


Fig. 4. The x_b - y_b - z_b body coordinate system and its spatial relation to the original x - y - z coordinate system.

radially directed x_b -axis forms angle Ψ against the x - y plane while the y_b -axis is always confined in the same plane. Consequently, the discoid body coaxially rotates around the z_b -axis at angular velocity ω in the x_b - y_b plane.

Transformation of the acceleration from the original x - y - z coordinate system to the x_b - y_b - z_b body coordinate system can be performed by the following equations:

$$\alpha_{x_b} = (\alpha_x \cos \theta + \alpha_y \sin \theta) \cos \Psi - \alpha_z \sin \Psi \quad (7)$$

$$\alpha_{y_b} = -\alpha_x \sin \theta + \alpha_y \cos \theta \quad (8)$$

$$\alpha_{z_b} = (\alpha_x \cos \theta + \alpha_y \sin \theta) \sin \Psi + \alpha_z \cos \Psi \quad (9)$$

which become

$$\alpha_{x_b} = -R\omega^2 [\cos \Psi - \beta (1 + \cos \Psi)^2 \cos \theta] \quad (10)$$

$$\alpha_{y_b} = R\omega^2 (1 + \cos \Psi) 2\beta \sin \theta \tag{11}$$

$$\alpha_{z_b} = -R\omega^2 \sin \Psi [1 - \beta(2 + \cos \Psi) \cos \theta] \tag{12}$$

For convenience of the diagrammatical expression of acceleration vectors, the first two components, α_{x_b} and α_{y_b} , are combined into a single vector and expressed as an arrow in the x_b - y_b plane, while the third vector, α_{z_b} , is separately expressed as a column. Fig. 5 illustrates distribution of centrifugal force vectors (the same magnitude as the acceleration but acting in the opposite direction) produced by the planetary motion at $\Psi = 25^\circ$.

In the diagram, the center of the discoid body coincides with the center of the x_b - y_b body coordinate system, where five concentric circles indicate location of arbitrary points at the labelled β values ($\beta = r/R$) of 0.1, 0.25, 0.5, 0.75 and 1.0 from

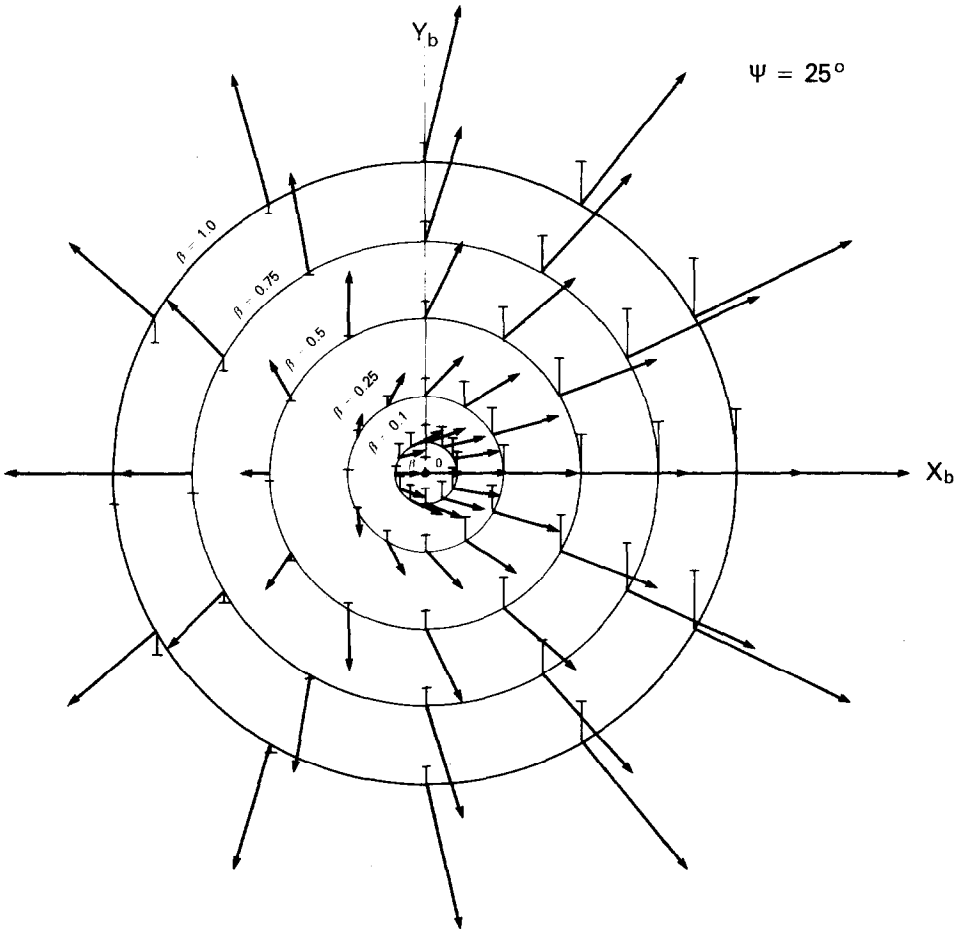


Fig. 5. Distribution of the centrifugal force vectors produced by the new synchronous planetary motion at $\Psi = 25^\circ$.

the center ($\beta = 0$) toward the periphery. On each circle, the centrifugal force vectors are drawn at every 30° -interval as two components. As mentioned earlier, the force component acting in the x_b - y_b plane is indicated by an arrow while the second component ($-\alpha_{z_b}$) acting perpendicularly to the x_b - y_b plane is expressed as a column in which the force pointing above the plane is shown by an ascending column and the force pointing below the plane by a descending column. Although the present diagram (Fig. 5) illustrates the centrifugal force field acting at a given moment, successive change of the force vector at a given point during revolution can be visualized easily either by moving the point counter-clockwise against the force field or by rotating the force field clockwise with respect to the point.

The overall picture of the centrifugal force distribution closely resembles that produced by the Scheme IV planetary motion as expected, except for the presence of the second component acting perpendicularly to the x_b - y_b plane. When the β value exceeds 0.25, force vectors always become directed outwardly from the circle while the second force component acts momentarily downward in the vicinity of the axis of revolution. As the β value becomes greater, force vectors increase their magnitude while reducing the amplitude of oscillation.

COMPARISON OF CENTRIFUGAL FORCE FIELD GENERATED BY ALL TYPES OF SYNCHRONOUS PLANETARY MOTIONS

Eqns. 10-12 derived from the above analysis can be applied universally for computing the acceleration produced from all types of synchronous planetary motions simply by substituting the corresponding angles for Ψ , *e.g.*, 180° for Scheme I, 90° for Scheme III and 0° for Scheme IV. Then, distribution of the centrifugal force vectors can be computed for each scheme and expressed in the same format as illustrated in Fig. 5 for $\Psi = 25^\circ$.

Fig. 6 illustrates a set of the centrifugal force distribution diagrams for five types of synchronous planetary motion. In the first column (left), more descriptive new terms are introduced for each type of synchronous planetary motion to replace the old terms indicated in parentheses. The second column gives the angle Ψ characteristic of each type of synchronous planetary motion. In the two hybrid types, Type I-L and Type J-L, Ψ is chosen at 135° and 45° , respectively, to facilitate comparative studies.

The third column in Fig. 6 illustrates orientation and planetary motion of the discoid body. It also indicates orientation of the x_b - y_b - z_b coordinate system, which serves as a reference frame for the force distribution diagram shown in the next column. The orientation of the x_b - y_b - z_b body coordinate system is selected in such a way that the z_b force component acting upward from the discoid body is always indicated as an ascending column in the force distribution diagram, except for the transitional angle of $\Psi = 90^\circ$ where the z_b force component acting radially from the center of revolution toward the periphery (right) is expressed as the ascending column. Accordingly, the orientation of the reference frame is corrected by rotating the x_b - y_b - z_b coordinate frame around the y_b -axis by 180° for $\Psi > 90^\circ$. This transposition also causes conversion of the $+/-$ signs for the x_b force component to normalize the direction of the x_b - y_b force vector expressed as an arrow in the force distribution diagram.

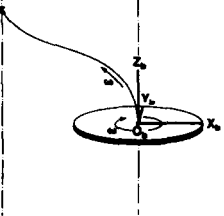
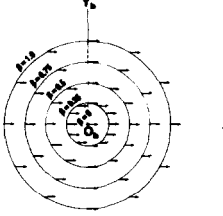
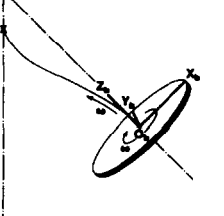
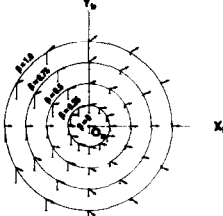
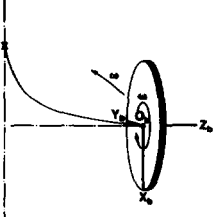
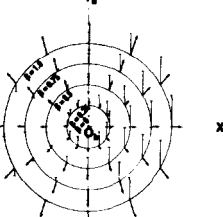
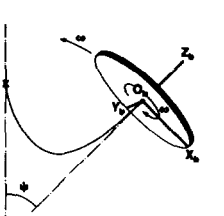
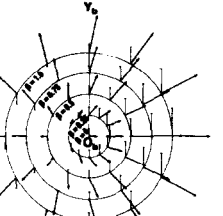
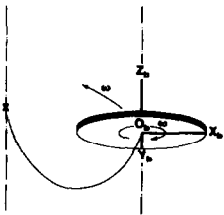
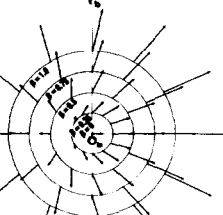
New Nomenclature of Synchronous Planetary Motion (Old Terms)	Angle ψ	Planetary Motion and Reference Coordinate Frame	Force Distribution Diagram
Type I (Scheme I)	180°		
Type I-L (Scheme II)	135°		
Type L (Scheme III)	90°		
Type J-L	45°		
Type J (Scheme IV)	0°		

Fig. 6. A set of the centrifugal force distribution diagrams for five types of synchronous planetary motion

In the fourth and the final column in Fig. 6 (right), the distribution of the centrifugal force vectors is displayed for various Ψ values in the order from 180° (top) to 0° (bottom) using the reference body coordinate frame indicated in the third column. As described earlier, all these force distribution diagrams are computed from a set of eqns. 10–12 by inserting the respective Ψ values indicated in the second column. In order to facilitate comparison, the length of the arrows and the columns which represent the magnitude of the force vector is normalized on the basis of the unit ($R\omega^2$) used in the first diagram ($\Psi = 180^\circ$) so that the lengths of vectors drawn in these diagrams accurately represent the relative magnitude of the force generated by the respective planetary motion at the same revolutional radius (R) and angular velocity (ω).

Observation of the force distribution diagrams from the top through to the bottom reveals successive changes in the distribution patterns of the first force component (arrows), while distribution of the second force component acting along the z_b -axis (columns) shows disruption of the continuity between $\Psi = 135^\circ$ and 90° due to the transposition of the x_b - y_b - z_b reference frame as described earlier. At $\Psi = 180^\circ$, the diagram shows homogeneous two-dimensional distribution of the centrifugal force vectors, each component measuring a unit length and acting in the same direction parallel to the radius of revolution. At $\Psi = 135^\circ$, the force distribution becomes three-dimensional: the first component (arrow) shows somewhat diverged distribution with slight decrease in magnitude, while the second component (column) acts strongly downward on the left and slightly upward on the right. When Ψ reaches the transitional angle of 90° , the first force component (arrow) forms symmetrical distribution always acting outwardly from the circle, while the second force component (column) acts very strongly upward (or toward the periphery along the radius of revolution) on the right. Here, it is interesting to note that the second force component also acts downward on the left, indicating that the centrifugal force is momentarily directed toward the center of revolution at the very top of the discoid body. This strange phenomenon, which has been reported elsewhere⁴, is explained on the basis of the Coriolis force produced by the planetary motion. As Ψ is further decreased to 45° , the first force component (arrow) remarkably gains the strength, especially on the right, while the second component (column) maintains the similar profile. Finally, at $\Psi = 0^\circ$, the distribution of the force vectors returns to the two-dimensional pattern as in the first diagram ($\Psi = 180^\circ$), but it consists of a complex arrangement of force vectors diverging from each circle with a great enhancement of the magnitude, especially at the remote location from the center of the discoid body.

Comparison between the two extreme types of synchronous planetary motion, Type I and Type J, reveals a remarkable difference in both the distribution pattern and magnitude of the centrifugal force vectors under the same revolutional speed and radius. The above difference is clearly manifested in the hydrodynamic effects on the two immiscible solvent phases in the coiled column. As briefly mentioned earlier, the Type I planetary motion produces the basic hydrodynamic equilibrium where the two solvent phases are evenly distributed in the coiled column from the head toward the tail, while any excess of either phase remains at the tail. This hydrodynamic distribution of the two solvent phases can be utilized for performing CCC by introducing the mobile phase through the head of the coiled column. However, in this mode of elution the stationary phase volume retained in the column is

substantially less than 50% of the total column capacity. On the other hand, the Type J planetary motion distributes the two solvent phases unilaterally in the rotating coil (coaxially mounted on the holder), where one phase entirely occupies the head side and the other phase the tail side. As previously described⁵⁻⁸, this unilateral hydrodynamic distribution is capable of retaining a large volume of the stationary phase in the column and is considered to be ideal for performing CCC. Under a proper elution mode and flow-rate of the mobile phase, the retention of the stationary phase often exceeds 80% of the total column capacity. Recently, hydrodynamic motion of the two solvent phases produced by this type of planetary motion has been observed under stroboscopic illumination⁹. The experiments revealed two distinct zones in each turn of the spiral column, a mixing zone of *ca.* a quarter turn located near the center of the centrifuge and a settling zone showing a clear interface of the two phases in the rest of the column. The high-partition efficiency characteristic of high-speed CCC may be largely attributed to this local mixing unique to the Type J synchronous planetary motion.

The hydrodynamic effects produced by three other types of synchronous planetary motions have not been reported, except for some observation on the retention and mixing capability in analytical columns^{3,4,10}. However, the force distribution diagrams of the two hybrid types, Type I-L and Type J-L, bear a strong resemblance to the pattern produced by each parent scheme described above, except for the additional force field acting along the z_b -axis which would introduce three-dimensional mixing of the solvents. Therefore, it is reasonable to assume that these two hybrid types illustrated in Fig. 6 would produce characteristic hydrodynamic effects as demonstrated by the respective parent schemes, *i.e.*, the Type I-L planetary motion would establish the basic hydrodynamic equilibrium of the two immiscible solvents, and the Type J-L planetary motion, the unilateral hydrodynamic equilibrium. If this is the case, one can expect superior results from the Type J-L coil planet centrifuge to the type I-L in performing CCC. As previously demonstrated by the angle rotor coil planet centrifuge (Type I-L)³, the force field acting along the z_b -axis could be utilized to produce beneficial effects on retention and mixing of the solvents by optimizing the orientation and configuration of the coiled column on the holder, thus adding great versatility to the system.

In the light of the above discussion, it may be of interest to build a new Type J-L angle rotor coil planet centrifuge and examine the various hydrodynamic effects of its centrifugal force field elucidated in this paper.

REFERENCES

- 1 Y. Ito, *J. Biochem. Biophys. Methods*, 5 (1981) 105.
- 2 Y. Ito and R. L. Bowman, *Science (Washington, D.C.)*, 173 (1971) 420.
- 3 Y. Ito and R. L. Bowman, *Anal. Biochem.*, 65 (1975) 310.
- 4 Y. Ito, R. L. Bowman and F. W. Noble, *Anal. Biochem.*, 49 (1972) 1.
- 5 Y. Ito, *J. Chromatogr.*, 207 (1981) 161.
- 6 Y. Ito, J. L. Sandlin and W. G. Bowers, *J. Chromatogr.*, 244 (1982) 247.
- 7 Y. Ito and R. Bhatnagar, *J. Liq. Chromatogr.*, 7 (1984) 257.
- 8 Y. Ito, *Adv. Chromatogr. (N.Y.)*, 24 (1984) 181.
- 9 W. D. Conway and Y. Ito, *Pittsburgh Conference and Exposition on Analytical Chemistry and Applied Spectroscopy*, No. 472, 1984, p. 472.
- 10 Y. Ito and R. L. Bowman, *Science (Washington, D.C.)*, 182 (1973) 391.